Fe doped TiO_2–graphene nanostructures: synthesis, DFT modeling and photocatalysis

2014 Nanotechnology 25 305601

(http://iopscience.iop.org/0957-4484/25/30/305601)

IOP Publishing Nanotechnology
Nanotechnology **25** (2014) 305601 (11pp) doi:10.1088/0957-4484/25/30/305601

Fe doped TiO_2–graphene nanostructures: synthesis, DFT modeling and photocatalysis

Nasrin Farhangi, Serge Ayissi and Paul A Charpentier

Department of Chemical and Biochemical Engineering, University of Western Ontario, London, Ontario, Canada N6A5B9

E-mail: pcharpentier@eng.uwo.ca

Received 4 March 2014, revised 21 May 2014
Accepted for publication 27 May 2014
Published 8 July 2014

Abstract

In this work, Fe-doped TiO_2 nanoparticles ranging from a 0.2 to 1 weight % were grown from the surface of graphene sheet templates containing –COOH functionalities using sol–gel chemistry in a green solvent, a mixture of water/ethanol. The assemblies were characterized by a variety of analytical techniques, with the coordination mechanism examined theoretically using the density functional theory (DFT). Scanning electron microscopy and transmission electron microscopy images showed excellent decoration of the Fe-doped TiO_2 nanoparticles on the surface of the graphene sheets >5 nm in diameter. The surface area and optical properties of the Fe-doped photocatalysts were measured by BET, UV and PL spectrometry and compared to non-graphene and pure TiO_2 analogs, showing a plateau at 0.6% Fe. Interactions between graphene and Fe-doped anatase TiO_2 were also studied theoretically using the Vienna *ab initio* Simulation Package based on DFT. Our first-principles theoretical investigations validated the experimental findings, showing the strength in the physical and chemical adsorption between the graphene and Fe-doped TiO_2. The resulting assemblies were tested for photodegradation under visible light using 17β-estradiol (E2) as a model compound, with all investigated catalysts showing significant enhancements in photocatalytic activity in the degradation of E2.

Keywords: Fe doped TiO_2, graphene, photocatalysis, DFT, estradiol

(Some figures may appear in colour only in the online journal)

1. Introduction

Control of environmental contamination is a current critical challenge, particularly wastewater pollution with growing concentrations of endocrine disrupting hormones. Heterogeneous photocatalysis using TiO_2, is of particular interest as an efficient method for water purification [1–4]. Titania has a number of useful properties including being non-toxic, biocompatible, inexpensive, and thermodynamically stable. It has been shown to be efficient for the degradation of hazardous aromatic molecules in polluted water and air [5]. However, it is generally recognized that the TiO_2 crystal structure needs to be modified to obtain its maximum efficiency as it has a large band gap and its photocatalytic efficiency is rather low [6]. Doping is a common method to extend the band gap of TiO_2 into the visible region [7–10] with numerous ions of transition metals investigated as potential dopants [11–13]. Among those, Fe^{3+} is considered as a good candidate as it can easily fit into the crystal lattice of TiO_2 and has a similar radius and redox potential to Ti^{4+} [14–16].

TiO_2 nanoparticles agglomerate easily [17], their aggregation effects can be minimized when they are attached to the surface of different porous materials such as zeolites [18], silica [19], activated carbon [20–25] or carbon naotubes [26–32]. More recently, graphene is of great interest [33–36] due to its larger surface area and potentially higher photocatalytic efficiencies [37]. Highly porous graphene sheets have the capacity to absorb larger quantities of pollutants on their surface, and to provide selective adsorption for desired pollutants. Some functional groups such as alcohol and carboxylic acids can be remained on the graphene surface during synthesis process [38], allowing for both adsorption of specific pollutants and attachment sites for nanoparticles to the graphene surface. Hence, different semiconductors can be

stabilized on its surface to produce more efficient photocatalysts [39, 40].

The ability to control nanocrystal growth from graphene's surface is still under active examination, with many results from different research studies inconsistent due to a large variation of experimental conditions investigated. In addition, very few reports investigate theoretically the interaction of nanoparticles and graphene sheets and the mechanism of charge transfer from graphene to the nanocrystal. In our previous studies, we decorated the surface of graphene with both TiO_2 nanofibers [41] and Fe doped TiO_2 nanofibers [42] in supercritical carbon dioxide ($scCO_2$) showing high phoyocatalitic properties. We also theoretically investigated both physical and chemical interaction of TiO_2 and graphene sheets using density functional theory (DFT) resulting in good charge transfer between graphene and TiO_2 [43]. Das *et al* deposited different semiconductor nanoparticles such as TiO_2 and ZnO and some magnetic nanoparticles such as Fe_3O_4 and Ni on graphene. By using first principle calculations, they showed that charge transfer occurs between graphene and the deposited nanoparticles [44]. Rojas *et al* used DFT calculations for Titanium modified graphene system for the adsorption of different molecules, showing considerably improved hydrogen storage capacity [45]. Herein, we synthesize different weight ratios of Fe-doped TiO_2 nanoassemblies ranging from 0.2 to 1% on the surface of graphene sheets using a sol–gel method in water/ethanol. The materials are characterized in detail and DFT calculations are examined to investigate the adsorption of the Fe doped TiO_2 nanocrystals to graphene and the energy transfer mechanism. Finally, the resulting materials are investigated for degradation of estrodine (E2) under visible light with the results compared to catalysts prepared in identical conditions without graphene.

2. Experimental

2.1. Materials

Graphite flakes nominally sized at 7–10 microns were provided from Alfa Aesar. Fuming nitric acid (>90%), sulfuric acid (95–98%), potassium chlorate (98%), hydrochloric acid (37%), acetic acid, titanium isopropoxide (99.999%) trace metals basis and iron chloride $FeCl_3$, were purchased from Sigma-Aldrich (Canada Ltd, Oakville, ON) and used as received.

2.2. Methods

2.2.1. Preparation of functionalized graphene sheets (FGSs). Staudenmaier method was used to produce graphene from graphite oxide [46]. Graphite (5 g) was reacted with concentrated nitric (45 mL) and sulfuric acid (90 mL) with potassium chlorate (55 g). To avoid any sudden increase in temperature, the potassium chlorate was added slowly over 15 min and mixture was stirred for more than 72 h at room temperature. The mixture was added to water after completing the reaction, washed with a 5% solution of HCl, and water repeatedly until the pH of the filtrate was neutral. The dried graphite oxide was placed in a quartz boat and inserted into a tubular furnace preheated to 1050 °C and kept at this temperature for 30 s. The graphite oxide was reduced to FGSs.

2.2.2. Preparation of Fe doped TiO_2/graphene sheet composites. A simple sol–gel method was used in this study as reported by Hoffman *et al* [47]. Acetic acid was added to 50 ml of distilled water to adjust it's pH to 2.6. Previously, we studied different FGSs: TIP ratios and 1:20 was found as an optimum value ratio [41]. In this study, we used the same FGSs: TIP weight ratio. Graphene sheets (FGSs/TIP: 1:20) were added to this solution gradually over 10 min to avoid agglomeration. In the next step, the appropriate amount of Fe was dissolved in 2 ml ethanol and added to the graphene solution. In another beaker, TiO_2 sols were prepared by drop wise addition of 5 mL of an ethanolic TIP solution, which had been dissolved in 50 mL of absolute ethanol, into the first beaker. After continuously stirring for 24 h, the resulting transparent solution was evaporated using a rotary evaporator at 50 °C and washed with distilled water and dried in the oven (80 °C) overnight. The obtained powder was calcined at 450 °C for 2 h under air.

2.3. Characterization

Scanning electron microscopy (SEM) (Model LEO 1530) and transmission electron microscopy (TEM) (Model JEOL 2010F) were used to examine the morphologies of the samples. For SEM imaging, samples were prepared by applying the powder directly to a carbon adhesive tape. The powdered samples for TEM analysis, were dispersed in methanol by sonication and then placed on a copper grid covered with holey carbon film and dried by evaporation. X-ray powder diffractometer (Rigaku Miniflex XRD, TX, USA), fitted with a rotating sample holder, a scintillation counter detector and a divergent beam utilizing a Cu Kα source of x-rays ($\lambda = 1.5418$ Å) was used to analyze structural of the samples. Different Fe doped TiO_2 particles were also prepared on the graphene sheets with the fraction of rutile (X_R) calculated using the Scherrer equation [47]:

$$X_R\,(\%) = \left\{1 - \left(1{+}1.26\, I_R/I_A\right) - 1\right\} \times 100, \qquad (1)$$

where I_R and I_A are the x-ray intensities of the rutile (101) and anatase (110) peaks, respectively. Raman analysis was performed using a Kaiser optical system (RXN1-785) with 5 times exposure and 20 times accumulation. The X-ray photoelectron spectroscopy (XPS) analysis was carried out with a Kratos Axis Ultra spectrometer using a monochromatic AlK (alpha) source (15 mA, 14 kV). UV spectra were performed by (Shimadzu 3600) deuterium arc lamp and two different detectors (PMT, and PbS). In order to measure diffuse reflectance of these materials, an integrating sphere was utilized.

Table 1. Synthesis conditions, morphology, BET surface area, pore volume, and pore size distribution of Fe-doped TiO_2/functionalized graphene sheet composites.

Dopant	Calcination T (°C)	Rutile (%)	Bandgap (eV)	Surface area ($m^2\ g^{-1}$)	Color
TiO_2	450	0	3.2	50	White
TiO_2/FGSs	450	0	2.9	124	Gray
0.6 % Fe–TiO_2	450	0	2.6	68	Yellow
0.2% Fe–TiO_2/FGSs	450	0	2.9	130	Light yellow
0.4% Fe-TiO_2/FGSs	450	0	2.7	158	Light yellow
0.6% Fe doped TiO_2/FGSs	450	0	2.5	188	Yellow
0.6% Fe–TiO_2/FGSs	700	53	2.5	98	Yellow
0.8% Fe–TiO_2/FGSs	450	0	2.5	190	Orange
1% Fe–TiO_2/FGSs	450	0	2.5	193	Orange

2.4. Photocatalytic activity measurements

17β-Estradiol (Sigma-Aldrich) was used as a model endocrine disrupting compound. In this experiment, the visible light source was a solar simulator (Model: SS1KW, Sciencetech) with a 1000 watt xenon arc lamp equipped with an air mass filter (AM filter) AM 1.5 G ($\lambda > 290$ nm) and a special UV cut-off filter ($290 \leqslant \lambda \leqslant 420$ nm). In a typical photodegradation experiment, a mixture of aqueous E2 solution (5 $\mu g\ L^{-1}$) and 0.5 $g\ L^{-1}$ of catalyst was vigorously stirred for 30 min to establish an adsorption/desorption equilibrium in the dark following by irradiation under visible light in an open water-jacketed vertical photo-reactor which was placed on a magnetic stirrer during all experiments, under aerated conditions [1]. Circulating cooling water was used to control the temperature of the reactions at 22 + 1 °C. At given time intervals, 5 mL aliquots were sampled and centrifuged to remove the particles. The supernatant was analyzed by HPLC using a (ICS 300, Dionex), which included a DP pump, an AS auto sampler, a dc column oven and PDA UV detector, connected to Chromeleon software. Separations were carried out with an Acclaim 120 C18 reversed-phase column (150 mm × 4.6 mm i.d., 5 μm particle size, Dionex, USA). The injection volume was 40 μL from a 2 mL HPLC vial, capped and sealed with PTFE lid. The mobile phase was the mixture of acetonitrile (AcN) and deionized water (Milli-Q) (50 : 50 v/v), delivered at a flow rate of 1 $mL\ min^{-1}$. The column temperature was maintained at 30 °C and detection wavelength was set at 280 nm which shows maximum absorbance of E2. The retention time of E2 in the HPLC column was 5.33 min. The measurements were repeated for each catalytic system, and the experimental error was found to be within (±1%).

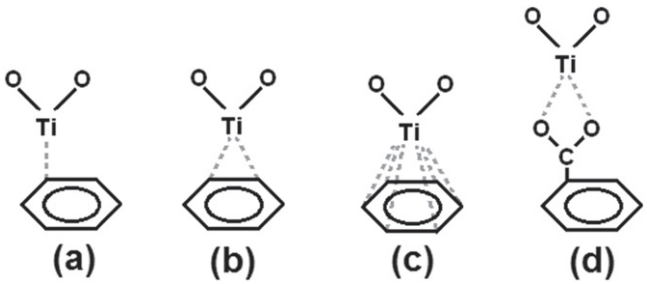

Scheme 1. Adsorption sites on pure and functionalized graphene substrates. TiO_2 adsorbates can possibly adsorb on (a) a top site, (b) a bridge site, (c) a hollow site of pure graphene and (d) a carboxylate site of functionalized graphene.

3. Computational methods

Theoretical bulk structures and binding energy values were studied using the Vienna *ab initio* Simulation Package (VASP) [48, 49] based on DFT. Electronic structure calculations were carried out using the GGA PW91 [50] functional implemented with VASP code for all graphene and titania systems. The electron–ion interactions are described by the projector-augmented wave scheme [49]. A constant energy cutoff of 400 eV was used for all the calculations for consistency in the bond length and angles. A Ti atom was substituted with a Fe atom in the 48-, 24- and 12-atom supercells to form the $Fe_xTi_{n-x}O_{2n}$ with the corresponding x doping values of 0.0625, 0.125 and 0.25 respectively, which represents the titania structures doped with uniformly distributed Fe atoms. A one-dimensional and periodic single sheet of 60 carbon atoms supercell passivated with hydrogens and organic groups have been used for the chemical adsorption (chemisorption) purposes. A two-dimensional and periodic single sheet of 100 carbon atoms supercell has been used for the description of physical adsorption (physisorption) phenomena. Four adsorption sites were considered: top, bridge, hollow sites on the pure graphene and carboxylate on the functionalized graphene. Schemes 1(a)–(d) show the schematic structures of titania species adsorbed on the possible sites of pure graphene and the carboxylate site of functionalized graphene.

4. Results and discussion

Different percentages of Fe doped TiO_2/FGSs were synthesized by a sol–gel method in a green solvent mixture of water and ethanol to give decorated graphene sheets. The experimental conditions and resulting properties of the synthesized materials are summarized in table 1.

Typical morphologies of the as-prepared FGSs are shown in figures 1(a) and (b) using SEM and TEM imaging. The SEM image of the FGSs shows the exfoliation of the reduced

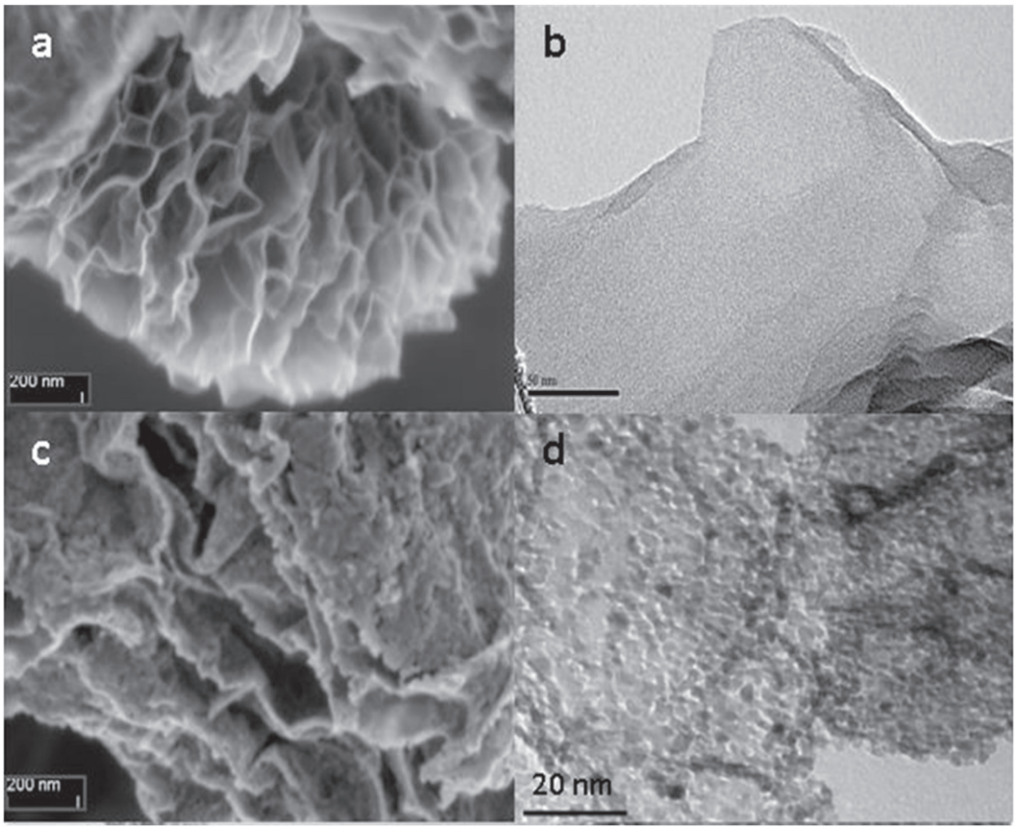

Figure 1. Functionalized graphene sheets (FGSs) (a) SEM, (b) TEM; 0.6% Fe doped TiO_2/FGSs (c) SEM and (d).

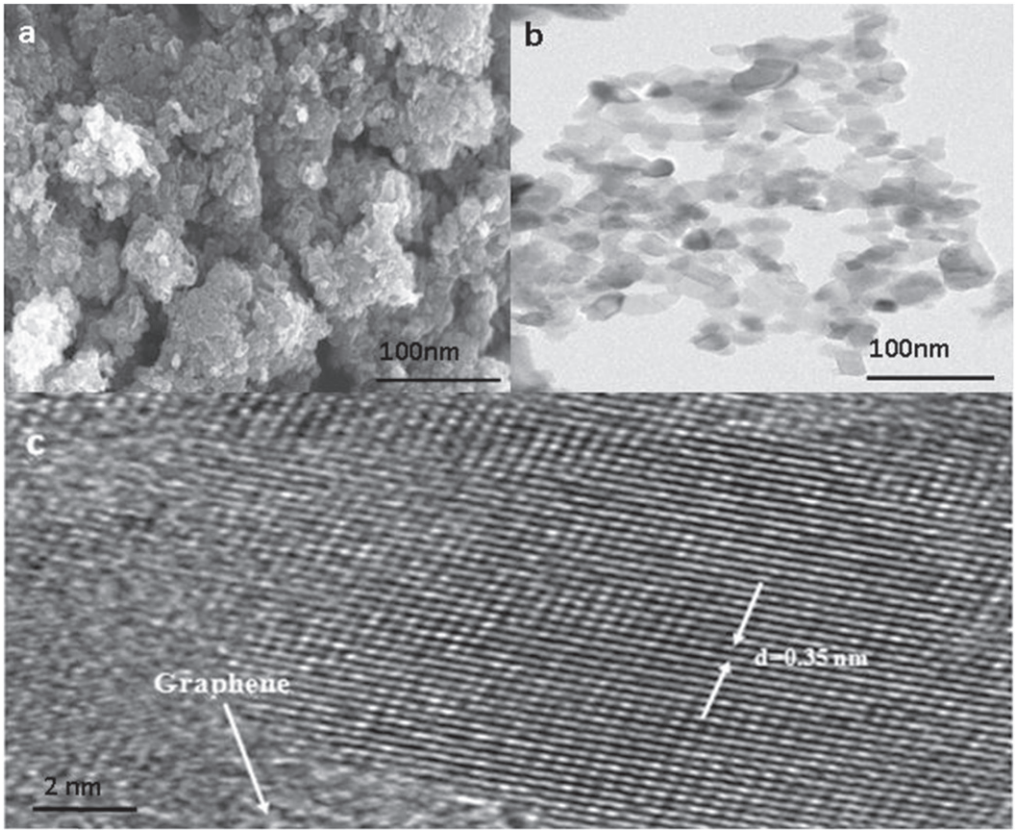

Figure 2. 0.6% Fe doped TiO_2 (a) SEM and (b) TEM, (c) HRTEM image of Fe doped TiO_2/FGSs (0.6%) calcined at 450 °C.

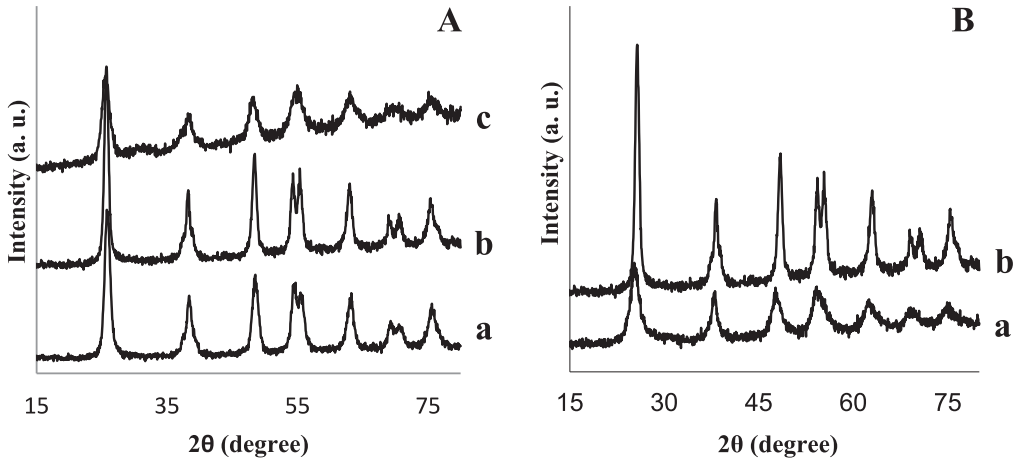

Figure 3. XRD spectra of (A) Fe doped 0.2% (a), 0.6% (b) and 1% (c), (B) 0.6 Fe doped TiO_2 (a), 0.6 Fe doped TiO_2/graphene (b) calcined at 450 °C.

graphite oxides and high porosity of the graphene sheets. A TEM image of the FGSs is shown in figure 1(b); here a thin paper-like structure is observed which is not completely flat showing wrinkles on the edges [51].

Most of the graphene sheets are very thin as has been previously observed; however some of them stack together due to van der Waals interactions. In figures 1(c) and (d), typical SEM and TEM images of the Fe-doped TiO_2 grown on the surface of graphene sheets is shown in which a uniform dispersion of small nanoparticles on the sheets is clearly observable. In the TEM images, doped TiO_2 nanoparticles less than 5 nm covered the entire surface of the graphene sheets with no significant agglomeration of nanoparticles detected. However, more nanoparticles are observed on the edges of the graphene sheets as darker spots are obvious on the graphene edges. This is attributed to a higher number of functional groups on that area as other researchers have shown [52]. Our calculations for both TiO_2 nanofibers on graphene sheets [43] and Fe doped TiO_2 nanoparticles on graphene (this paper) are also confirm the existence of strong chemisorptions between nanoparticles and –COOH groups on the edges of graphene sheets.

Typical SEM and TEM images of Fe doped TiO_2 are presented in figures 2(a) and (b). When graphene sheets were not used as a support, the size of TiO_2 particles significantly increased up to 50 nm and some of the particles agglomerated. Hence, it is apparent that the graphene sheets can facilitate uniform dispersion of the nanoparticles on its surface while controlling their size. As described in detail below, doped TiO_2 particles grown from carboxyl groups on the surface of the graphene sheets, significantly decrease the degree of agglomeration. A HRTEM micrograph of the lattice image of 0.6% Fe doped titania/graphene calcined at 450 °C is given in figure 2(c), showing uniform dispersion of anatase with d-spacing 0.35 nm (101) [53]. There was no Fe detected in the HRTEM micrographs, indicating that all the Fe is impregnated within the TiO_2 lattice. Some amorphous regions are also observable, corresponding to the presence of graphene sheets in the composites.

The BET surface areas provided in table 1 were determined using nitrogen adsorption and desorption isotherms. Synthesized FGSs showed high surface areas (1100 $m^2\,g^{-1}$) while the BET surface area of the undoped sol–gel synthesized TiO_2, which was calcined at 450 °C, was found to be 85 $m^2\,g^{-1}$. The BET surface areas of the Fe-doped TiO_2 samples were found to be slightly larger than the undoped TiO_2 (105 $m^2\,g^{-1}$). When Fe-doped TiO_2 was grown on the surface of the graphene sheets, the surface area increased to 180 $m^2\,g^{-1}$. By increasing the amount of Fe in the composites, the surface area was enhanced (230 $m^2\,g^{-1}$ for 0.6% Fe doped/TiO_2/FGSs), which is attributed to producing more pores inside the composites. By increasing the calcination temperature to 700 °C, the surface area decreased to 70–112 $m^2\,g^{-1}$ which is attributed to the agglomeration of TiO_2 nanoparticles and the collapse of the porous structure.

The FGSs did not show any peaks in XRD which means that either all stacking is lost or the remaining stacking is disordered [54]. Figure 3(A) shows the XRD patterns of different amounts of Fe-doped TiO_2/FGSs composites calcined at 450 °C. All spectra show anatase phase, however the crystallinity varies. By increasing the amount of Fe from 0.2 to 0.6%, the crystallity increases, whereas further increasing to 1% decreases the crystallity probably because of excess amount of Fe which can not properly fit inside the TiO_2 crystal. In figure 3(B), the XRD patterns of Fe doped TiO_2 (0.6%) with and without graphene are compared. The crystallinity is significantly higher when grown on the FGSs. In explanation, when Fe doped TiO_2 nanostructures were grown on the surface of the graphene sheets, the functional groups on the graphene sheets acted as templates, enhancing crystallization and resulting in smaller sized TiO_2 nanocrystals being obtained.

Diffuse reflectance UV–Vis spectroscopy was applied to further study the interactions between the Fe doped TiO_2 and graphene in the composites. The UV–Vis spectra indicates that Fe doped TiO_2/graphene gave strong absorbance in the UVA-visible region (300–700 nm) with the band gap decreasing to 2.5 eV, as calculated using the basic energy

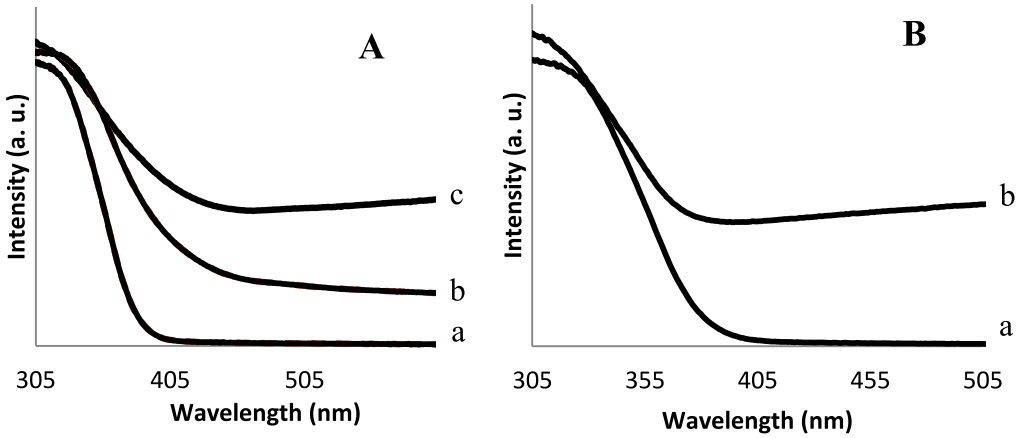

Figure 4. Diffuse reflectance UV–Vis spectra of: (A) (a) TiO_2 anatase; (b) 0.4% Fe doped TiO_2 and (c) 0.4% Fe doped TiO_2/FGSs; (B) (a) TiO_2 anatase, (b) TiO_2/FGSs.

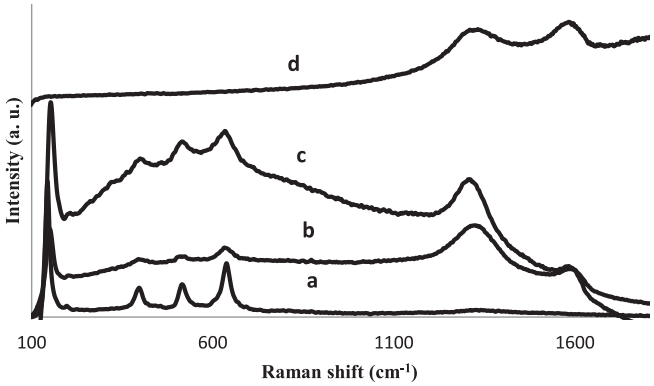

Figure 5. Raman spectrum of TiO_2 (a) Fe doped TiO_2/FGSs (0.2%) (b), Fe doped TiO_2 (0.8%) (c), and functionalized graphene sheets (FGSs) (d).

equation ($E = hc/\lambda$) (table 1). Different studies on TiO_2/graphene composites have shown that graphene can narrow the band gap of TiO_2 [36, 55, 56]. Formation of Ti–O–C bonding between TiO_2 and graphene sheets, similar to that observed with carbon-doped TiO_2 composites, is a potential reason for the red shift in the UV spectra [57].

Metal-doping enhances visible light absorption owing to the formation of intermediate energy levels, leading to a decrease in the energy band gap [58]. Figure 4(A) compares the UV spectra of Fe-doped TiO_2 with and without graphene sheets. By adding graphene to the system, the band gap of Fe doped TiO_2 decreased from 2.6 to 2.5 eV, which helps confirm that graphene acts as a photosensitizer. In figure 4(B), the UV spectra of TiO_2 with band gap of 3.2 eV is compared to TiO_2/FGSs with a band gap of 2.9 eV.

Graphene has two characteristic peaks in the Raman spectra; (figure 5(d)) i.e. a broad D and G band, which are assigned to the C sp^2 atoms and one to C sp^3 atoms, respectively [59]. After functionalization of graphene with TiO_2, the intensity ratio of the D band to G band, which is proposed as an indication of disorder in the prepared catalysts, increased dramatically indicating good attachment of the TiO_2 nanoparticles to the graphene surface. All doped TiO_2/FGSs samples calcined at 450 °C are present in the anatase phase, corresponding to characteristic peaks around 143 cm^{-1}, which are attributed to the main E_g anatase vibration mode. Crystalline TiO_2 showed the vibration peaks at 400 cm^{-1} (B_{1g}), 519 cm^{-1} (A_{1g}) and 640 cm^{-1} (E_g) as well [60]. The Raman spectra of the prepared Fe-doped TiO_2/FGSs are shown in figures 5(b), (c) which is in good accordance with the XRD patterns as no Fe peak is detected. The peak position shifts towards a higher wavenumber in the order of 0.2 and 0.8% Fe doped TiO_2/FGSs, indicating an increase in the number of surface oxygen vacancies. The more oxygen vacancies induced by Fe-doping could be attributed to the incorporation of Fe-dopants into the TiO_2 lattice. Zhu *et al* Fe-doped nanocrystalline was prepared by Zhu *et al* via a non-hydrolytic sol–gel method and showed the same shift in the Raman study [61].

To further investigate nanoparticle linking to graphene, XPS was examined. The XPS spectra of 0.6% Fe doped TiO_2/FGSs shows 6.1% Fe 2p, 54.7% O1s, 18.7% Ti 2p and 20.5% C1s (figure 6).

In the high resolution of C1s, the intensity of C=O and C–OH peaks decreased compared to those of FGSs. Coordination between Ti and carboxylic acids on the surface of the graphene sheets resulted in a shift of C=O peak which is located at 289.25 eV to a lower energy value (288.8 eV). The O 1s showed a main peak at 530.3 eV which is assigned to the (Ti–O). Hyroxyl group showed a peak at 533.4 eV in FGSs. This peak disappeared after functionalization of FGSs with Fe doped TiO_2 , but the peak at 531.4 eV corresponding to the carbonyl group is still available [62]. As shown in figure 7, two peaks at 458.4 eV and 464.1 eV which are consistent with the values of Ti^{4+} in the TiO_2 lattices represent the Ti 2p3/2 and Ti 2p1/2 for Fe doped TiO_2 on the graphene surface [63]. Fe^3 (2p3/2 and 2p1/2) also represent peaks at 711.9 eV and 724.6 eV , respectively which exhibit a slightly positive shift compared to those in Fe_2O_3 (710.7 eV for 2p3/2 and 724.3 eV for 2p1/2) due to formation of Fe–O–Ti bonding and transferring the electrons from Fe^{3+} into the TiO_2 lattice [63]. We observed similar results when comparing Fe-doped TiO_2/FGSs nanowires prepared using $scCO_2$ [42].

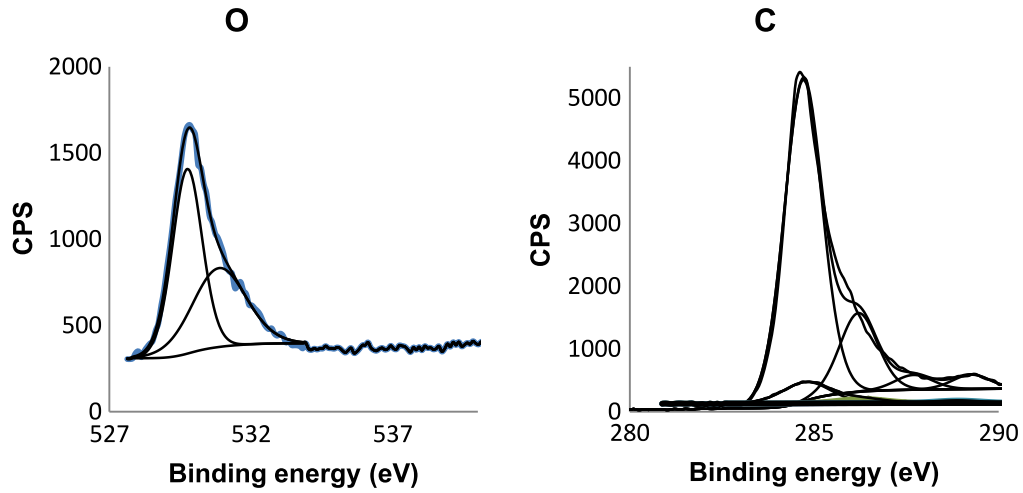

Figure 6. XPS spectra of FGSs, high resolution (a) C (1s) and (b) O (1s).

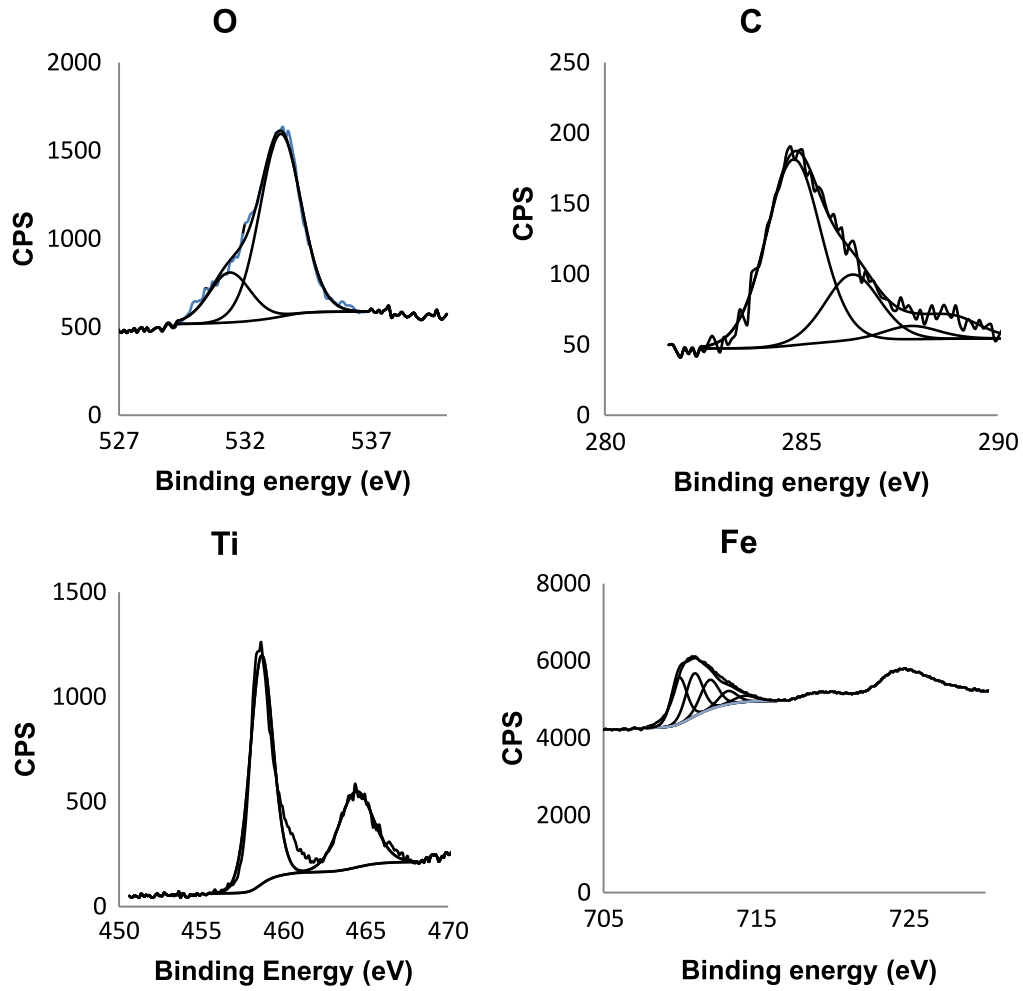

Figure 7. XPS spectra of 0.6% Fe doped TiO_2/FGSs, high resolution (a) O, (b) C, (c) Ti and (d) Fe.

5. Theoretical calculations of adsorption and energy transfer

Presently, only a few theoretical studies exist on the interactions of TiO_2 and graphene sheets [64]. However, most of these studies have only focused on ideal graphene sheets (periodic and infinite supercells), without any functional groups or defective sites interacting with gas phase or molecular TiO_2. We recently studied the interaction of small size titania nanostructures with pure and functionalized graphene by DFT [43]. Hence, here we investigate the interactions of Fe doped TiO_2 when in direct contact with

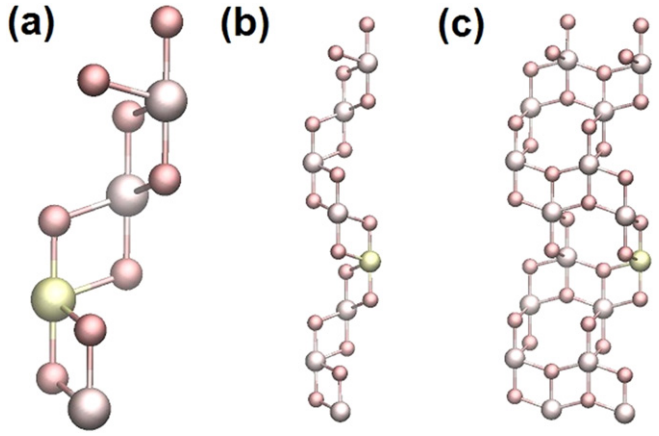

Figure 8. Schematic structure of Fe-doped anatase TiO_2 nanostructures. By the substitution of a Ti atom with Fe on a 12, a 24 and a 48-atom unit cell of anatase titania we obtain respectively (a) $FeTi_3O_8$, (b) $FeTi_7O_{16}$ and (c) $FeTi_{15}O_{32}$ compounds.

pure and FGSs, comparing the results with our recent study of undoped rutile and anatase TiO_2 nanostructures [43]. An initial unit cell of anatase TiO_2 (Ti_4O_8) was used doped with a Fe cation, which can be can be placed in 4 different positions of the unit cell. The study was extended adding two Fe-doped anatase TiO_2 adsorbates with much lower doping concentration. Scheme 1 shows the schematic structure of Fe-doped anatase titania adsorbates used for chemical and physical adsorption on graphene. A 12-atom adsorbate of 0.25 concentration value was initially used followed by a 24-atom of a 0.125 concentration and a 48-atom nanostructure of 0.0625 concentration were used to complete the adsorption study. The $FeTi_3O_8$ TiO_2 unit cell was initially calculated in a small rectangular supercell ($3.29 \times 3.29 \times 10.27$ Å^3) for a structural optimization of its bulk properties. Then the isolated nanostructure had its wavefunction optimized in a large rectangular supercell ($21.2 \times 12.3 \times 30.0$ Å^3). The same ground states set up was applied to the $FeTi_7O_{16}$ nanostructures which was initially calculated in a rectangular unit cell of ($3.26 \times 3.26 \times 20.02$ Å^3) and to the $FeTi_{15}O_{32}$ nanostructure in a ($3.23 \times 6.58 \times 20.02$ Å^3) unit cell. Spin polarization was considered in all calculations, and the electronic structures were optimized to their ground states.

Figure 8 shows three unit cells of Fe doped anatase at different concentration and specifically where the Fe atom was doped within the anatase TiO_2 structure. Pink spheres represent the titanium atoms, yellow spheres the iron atom and red spheres the oxygen atoms. From the XPS results, we chose ($x = 1$) as the unit cell, which corresponds to the formula $FeTi_3O_8$, $FeTi_7O_{16}$ and $FeTi_{15}O_{32}$ and respectively to concentrations of 25%, 12% and 6% (w%) cation doping of anatase. Note that the Fe atom is not involved in binding to the graphene sheet, as the Fe-doping only plays a role in the electronic structure of anatase. Titanium binds to the clean and FGS in all cases of physisorption and chemisorption. These adsorption sites are the top, the bridge, the hollow, and the carboxylate site. Schemes 1(a), (b) and (c) show these three types of physical adsorptions (physisorption) while Scheme 1(d) shows the unique chemical adsorption (chemisorption) site. If anatase TiO_2 is rotated by 90° on graphene, it results in a rotated adsorption site that may lead to slightly different results, as previously discussed [43].

Table 2. Calculated binding energy values for Fe-doped anatase TiO_2 nanostructures adsorbed on graphene substrates.

	$FeTi_3O_8$		$FeTi_7O_{16}$		$FeTi_{15}O_{32}$	
Adsorption sites	E_b (eV)	Ti–C (Å)	E_b (eV)	Ti–C (Å)	E_b (eV)	Ti–C (Å)
Top	1.774	2.20	1.845	2.21	1.874	2.18
Bridge	1.742	2.32	1.649	2.28	1.759	2.33
Hollow	2.201	2.47	2.222	2.42	2.398	2.40
Carboxylate	5.785	1.94	5.623	1.96	5.380	1.97

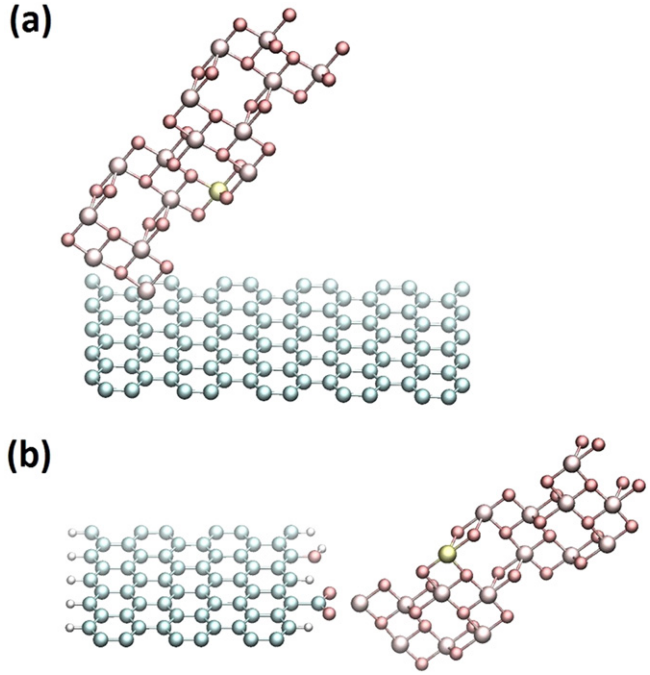

Figure 9. Physisorption and chemisorption of anatase titania on graphene and functionalized graphene substrates. $FeTi_{15}O_{32}$ adsorbs successfully on (a) a top site of pure graphene and (b) a carboxylate site of functionalized graphene.

All binding energy values of anatase TiO_2 adsorbed on graphene are presented in table 2.

Figure 9 shows a typical adsorption study of titania nanostructures adsorbed on graphene substrates, figure 9(a) $FeTi_{15}O_{32}$ physisorbed on pure graphene and figure 9(b) $FeTi_{15}O_{32}$ chemisorbed on functionalized graphene. A 100 carbon atom supercell was used for the physisorption study (figure 9(a)), while a 60 carbon atom supercell terminated by hydrogens, alcohol and carboxylates groups was used for the chemisorption study (figure 9(b)). The adsorption energy can

be calculated using the following equation:

$$E_b = E\,(\text{graphene}) + E\left(TiO_2\right) - E\left(TiO_2/\text{graphene}\right),$$

where E_b(or $E_{ads}(>0)$) represents the positive amount of binding energy. E(graphene) represents the total energy of the graphene sheet while $E(TiO_2)$ represents the total energy of the anatase (clean or doped) nanostructure. $E(TiO_2/\text{graphene})$ represents the total energy of a system in which both graphene and Titania are interacting. The adsorption energy was assumed to be favored when the binding energy was positive. For convenience, the binding energy E_b will be used in place of E_{ads} in the remaining sections [64].

A summary of the results for the optimized structures for all Fe-doped TiO_2/graphene systems is provided in table 2. Note that the physisorption is represented by Ti–C interactions and chemisorption by Ti–O interactions.

The three Fe-doped anatase nanostructures were successfully adsorbed on graphene and functionalized graphene on all the adsorption sites described in the above table 2. Fe-doped anatase TiO_2 is generally more favorable while adsorbed on graphene than pure anatase [43]. For all species, the chemical adsorption shows a higher binding energy compared to all physical adsorption sites. In terms of physisorption of Fe-doped titania on graphene, the hollow site shows a higher binding energy followed by the top site and the bridge site in every Fe-doped anatase nanostructure. As a result, Fe-doped anatase TiO_2 nanostructures are more likely to start their growth on the hollow sites of pure graphene.

As can be seen, the shortest separation between an atom of TiO_2 and the closest carbon atom of the graphene layer is between 2.19 and 2.45 Å in the case of physisorption and 1.92 Å for chemisorption. After doping TiO_2 with Fe, all distances increased by just 0.02 Å. Das *et al* deposited different nanoparticles such as TiO_2, ZnO, Fe_3O_4, and Ni on graphene surfaces and reports that the closest distances of graphene's carbon and nanoparticles range from 2.4 to 3.0 Å [44].

Interestingly, in physisorption, the relative binding energies are higher in all Fe-doped TiO_2 embedded in graphene than the corresponding undoped nanostructure, almost by 0.4 eV. The binding energy values remain stable with different sizes of Fe doped nano-adsorbates. It seems that when we replace one Ti atom with Fe, some magnetization in the composites occurs altering the charge transfer between the deposited nanoparticles and graphene. Das *et al* studied the interaction of graphene decorated by semiconducting and magnetic nanoparticles and found significant electronic and magnetic interactions facilitating charge transfer between the nanoparticles and graphene.

Higher binding energies with almost the same Ti–C bond distances helps confirm strong physisorption occurred between the Fe doped TiO_2 and the graphene sheets. Moreover, the binding energy in the presence of carboxylate groups on graphene results in slightly decreased chemisorption. However, the chemisorption value between the Fe doped TiO_2 and graphene surface was relatively strong, i.e. having a calculated bonding energy of roughly 5.50 eV.

Table 3. Visible-light photocatalytic activities of Fe-TiO_2 and Fe-TiO_2/FGSs samples for the degradation of E2.

Materials	k (h^{-1}) (calcined at 450 °C) first cycle	k (h^{-1}) (calcined at 450 °C) second cycle	k (h^{-1}) (calcined at 700 °C)
TiO_2	0.002	0.0015	0.0012
TiO_2/FGSs	0.003	0.0018	0.00176
0.2% Fe doped TiO_2	0.004	0.0032	0.0018
0.2% Fe doped TiO_2/FGSs	00.007	0.0054	0.0037
0.4% Fe doped TiO_2	0.0071	0.0052	0.00501
0.4% Fe doped TiO_2/FGSs	0.0091	0.0076	0.00721
0.6% Fe dopedTiO_2	0.0083	0.0059	0.00521
0.6%Fe doped TiO_2/FGSs	0.0123	0.0096	0.00892
0.8% Fe doped TiO_2	0.0087	0.0062	0.00592
0.8% Fe doped TiO_2/FGSs	0.0122	0.0093	0.00891

6. Visible light photocatalytic activity of Fe–TiO_2/FGSs

17β-estradiol (E2) was chosen as the model organic compound to evaluate the photoactivity of the prepared Fe doped TiO_2 nanoparticles on graphene sheets under visible light irradiation ($\lambda > 400$ nm). Photocatalytic degradation normally follows first-order kinetics:

$$\frac{dC}{dt} = -k_r \frac{K_a C}{1 + K_a C} \tag{3}$$

(dC/dt) is the degradation rate of E2, C is the concentration of E2 in the solution, t is reaction time, k_r is the reaction rate constant, and K_a is the adsorption coefficient of the reactant. When the value of C is very small, K_aC is negligible in equation (3). At $t=0$, $C=C_0$, it can be described as equation (4)

$$\ln\left(\frac{C_0}{C}\right) = K_{app} \times t. \tag{4}$$

The photocatalytic activities are shown in table 3, in which the observed rate constant was increased slightly to 0.003 h^{-1} in the presence of undoped TiO_2. However, Fe-TiO_2 showed significantly enhanced photocatalytic activities under the visible light irradiation. By increasing the amount of Fe in the composites from 0.4 to 0.6%, the rate constant increased from 0.0091 to 0.0123 h^{-1}. Further increasing the

amount of Fe to 0.8% did not affect the rate constant significantly ($k = 0.0123\ h^{-1}$), similar to the results obtained by UV–Vis. By preparing Fe–TiO_2 on the surface of graphene, the rate constant of E2 photodegradation increased significantly (table 2).

To examine recycling, all catalysts were filtered, then tested for the second cycle. Although the rate constants decreased, the catalysts were still active. Catalysts calcined at 700 °C were also tested for E2 photodegradation. The rate constant decreased significantly compared to catalysts calcined at 450 °C. This reduction should be because of catalyst sintering, i.e. collapsing the pores at high temperature and a subsequent decreasing of surface area as described above.

7. Conclusions

High performance Fe doped TiO_2 on the surface of graphene sheets were successfully synthesized via a simple sol–gel process in the green solvent mixture of water/ethanol. Fe–TiO_2/FGSs showed higher visible light absorption, higher surface areas than corresponding samples prepared without graphene. The prepared materials were examined for visible light degradation of E2—an endocrine disrupting hormone, which showed higher photocatalytic activity compared to TiO_2/graphene and metal doped TiO_2 composites. The observed photocatalytic enhancement can be explained by enhanced adsorptivity of dyes, extending the photoresponse range, and enhancing the charge separation and transportation properties simultaneously. DFT calculations were also performed, indicating possible physical interactions between Fe doped TiO_2 and graphene sheets on three different positions i.e. the top, the bridging and the hollow sites. The hollow sites were shown as the most stable configuration. Fe doped TiO_2/graphene composites showed higher stability than TiO_2/graphene composites because of higher charge transfer from the doped semiconductor to the graphene sheets. Fe doped TiO_2 decorated on carboxylated graphene sheets were also investigated which show strong chemical interactions between the Fe doped TiO_2 and graphene. These materials provide new possibilities in the investigation of TiO_2–graphene composites and promote their practical application in addressing various environmental issues.

References

[1] Matos J, Garcia A, Cordero T, Chovelon J-M and Ferronato C 2009 *Catal. Lett.* **130** 568–74
[2] Matos J, Laine J and Herrmann J-M 1998 *Appl. Catal. B: Environ.* **18** 281–91
[3] Herrmann J M, Matos J, Disdier J, Guillard C, Laine J, Malato S and Blanco J 1999 *Catal. Today* **54** 255–65
[4] Sato S 1986 *Chem. Phys. Lett.* **123** 126–8
[5] Navio J A, Colon G, Macias M, Real C and Litter M I 1999 *Appl. Catal.* A*: Gen.* **177** 111–20
[6] Rajh T, Ostafin A E, Micic O I, Tiede D M and Thurnauer M C 1996 *J. Phys. Chem.* **100** 4538–45
[7] Choi J, Park H and Hoffmann M R 2009 *J. Phys. Chem.* C **114** 783–92
[8] Choi W, Termin A and Hoffmann M R 1994 *J. Phys. Chem.* **98** 13669–79
[9] Wang Y, Wang Y, Meng Y, Ding H, Shan Y, Zhao X and Tang X 2008 *J. Phys. Chem.* C **112** 6620–6
[10] Sene J J, Zeltner W A and Anderson M A 2003 *J. Phys. Chem.* B **107** 1597–603
[11] Di Paola A, Garcia-López E, Ikeda S, Marci G, Ohtani B and Palmisano L 2002 *Catal. Today* **75** 87–93
[12] Sakthivel S, Shankar M V, Palanichamy M, Arabindoo B, Bahnemann D W and Murugesan V 2004 *Water Res.* **38** 3001–8
[13] Park M S, Kwon S K and Min B I 2002 *Phys. Rev.* B **65** 161201
[14] Wang J, Limas-Ballesteros R, Lopez T, Moreno A, Gomez R, Novaro O and Bokhimi X 2001 *J. Phys. Chem.* B **105** 9692–8
[15] Ambrus Z, Balazs N, Alapi T, Wittmann G, Sipos P, Dombi A and Mogyorósi K 2008 *Appl. Catal. B: Environ.* **81** 27–37
[16] Nagaveni K, Hegde M and Madras G 2004 *J. Phys. Chem.* B **108** 20204–12
[17] Gole J L, Stout J D, Burda C, Lou Y and Chen X 2003 *J. Phys. Chem.* B **108** 1230–40
[18] Reddy E P, Davydov L and Smirniotis P 2003 *Appl. Catal.* B*: Environ.* **42** 1–11
[19] Hirano M, Ota K and Iwata H 2004 *Chem. Mater.* **16** 3725–32
[20] Wang W, Silva C G and Faria J L 2007 *Appl. Catal.* B*: Environ.* **70** 470–8
[21] Torimoto T, Okawa Y, Takeda N and Yoneyama H 1997 *J. Photochem. Photobiol. A: Chem.* **103** 153–7
[22] Ao C H and Lee S C 2003 *Appl. Catal. B: Environ.* **44** 191–205
[23] Araña J, Doña-Rodríguez J M, Tello Rendón E, Garriga C, Cabo I, González-Díaz O, Herrera-Melián J A, Pérez-Peña J, Colón G and Navío J A 2003 *Appl. Cat. B: Environ.* **44** 161–72
[24] Fu P, Luan Y and Dai X 2004 *J. Mol. Catal. A: Chem.* **221** 81–8
[25] Zhang X, Zhou M and Lei L 2005 *Carbon* **43** 1700–8
[26] Jitianu A, Cacciaguerra T, Benoit R, Delpeux S, Béguin F and Bonnamy S 2004 *Carbon* **42** 1147–51
[27] Huang H, Zhang W K, Gan X P, Wang C and Zhang L 2007 *Mater. Lett.* **61** 296–9
[28] Moriguchi I, Hidaka R, Yamada H, Kudo T, Murakami H and Nakashima N 2006 *Adv. Mater.* **18** 69–73
[29] Jang S-R, Vittal R and Kim K-J 2004 *Langmuir* **20** 9807–10
[30] Yao Y, Li G, Ciston S, Lueptow R M and Gray K A 2008 *Environ. Sci. Technol.* **42** 4952–7
[31] Liu B and Zeng H C 2008 *Chem. Mater.* **20** 2711–8
[32] Gao B, Chen G Z and Li Puma G 2009 *Appl. Catal. B: Environ.* **89** 503–9
[33] Woan K, Pyrgiotakis G and Sigmund W 2009 *Adv. Mater.* **21** 2233–9
[34] Wang D, Choi D, Li J, Yang Z, Nie Z, Kou R, Hu D, Wang C, Saraf L V and Zhang J 2009 *ACS Nano* **3** 907–14
[35] Zhang H, Lv X, Li Y, Wang Y and Li J 2009 *ACS Nano* **4** 380–6
[36] Tang Y-B *et al* 2010 *ACS Nano* **4** 3482–8
[37] McAllister M J, Li J L, Adamson D H, Schniepp H C, Abdala A A, Liu J, Herrera-Alonso M, Milius D L, Car R and Prud'homme R K 2007 *Chem. Mater.* **19** 4396–404
[38] Schniepp H C, Li J L, McAllister M J, Sai H, Herrera-Alonso M, Adamson D H, Prud'homme R K, Car R, Saville D A and Aksay I A 2006 *J. Phys. Chem.* B **110** 8535–9

[39] Lightcap I V, Kosel T H and Kamat P V 2010 *Nano Lett.* **10** 577–83
[40] Kamat P V 2009 *J. Phys. Chem. Lett.* **1** 520–7
[41] Farhangi N, Medina-Gonzalez Y, Chowdhury R R and Charpentier P A 2012 *Nanotechnology* **23** 294005
[42] Farhangi N, Chowdhury R R, Medina-Gonzalez Y, Ray M B and Charpentier P A 2011 *Appl. Catal. B: Environ.* **110** 25–32
[43] Ayissi S, Charpentier P A, Farhangi N, Wood J A, Palotás K and Hofer W A 2013 *J. Phys. Chem.* C **117** 25424–32
[44] Das B, Choudhury B, Gomathi A, Manna A K, Pati S K and Rao C N R 2011 *Chem. Phys. Chem.* **12** 937–43
[45] Rojas M I and Leiva E P M 2007 *Phys. Rev.* B **76** 155415
[46] Staudenmaier L 1898 *Ber. Dtsch. Chem. Ges.* **31** 1481
[47] Choi J, Park H and Hoffmann M R 2010 *J. Phys. Chem.* C **114** 783–92
[48] Kresse G and Furthmüller J 1996 *Comput. Mater. Sci.* **6** 15–50
[49] Kresse G and Joubert D 1999 *Phys. Rev.* B **59** 1758–75
[50] Perdew J P, Chevary J A, Vosko S H, Jackson K A, Pederson M R, Singh D J and Fiolhais C 1992 *Phys. Rev.* B **46** 6671–87
[51] Schniepp H C, Li J-L, McAllister M J, Sai H, Herrera-Alonso M, Adamson D H, Prud'homme R K, Car R, Saville D A and Aksay I A 2006 *J. Phys. Chem.* B **110** 8535–9
[52] Wang D C *et al* 2009 *ACS Nano* **3** 907–14
[53] Miao L, Jin P, Kaneko K, Terai A, Nabatova-Gabain N and Tanemura S 2003 *Appl. Surf. Sci.* **212-213** 255–63
[54] Wang G, Yang J, Park J, Gou X, Wang B, Liu H and Yao J 2008 *J. Phys. Chem.* C **112** 8192–5
[55] Zhang Y, Tang Z-R, Fu X and Xu Y-J 2010 *ACS Nano* **4** 7303–14
[56] Zhang L X H *et al* 2010 *ACS Nano* **4** 380–6
[57] Park J H, Kim S and Bard A J 2005 *Nano Lett.* **6** 24–8
[58] Eder D, Motta M and Windle A H 2009 *Nanotechnology* **20** 055602
[59] Kudin K N, Ozbas B, Schniepp H C, Prud'homme R K, Aksay I A and Car R 2008 *Nano Lett.* **8** 36–41
[60] Zhang W F and Chen Q 2000 *J. Phys. D: Appl. Phys.* **33** 912–6
[61] Zhu J, Ren J, Huo Y, Bian Z and Li H 2007 *J. Phys. Chem.* C **111** 18965–9
[62] Akhavan O 2010 *Carbon* **48** 509–19
[63] Nagaveni K, Hegde M S and Madras G 2004 *J. Phys. Chem.* B **108** 20204–12
[64] Valencia H, Gil A and Frapper G 2010 *J. Phys. Chem.* C **114** 14141–53